LASER & PHOTONICS REVIEWS
www.lpr-journal.org

Nonlinear Generation, Compression and Spatio-Temporal Analysis of sub-GV/cm-Class Femtosecond Mid-Infrared Transients

*Christoph Schoenfeld, Lennart Feuerer, Alexander-Cornelius Heinrich, Alfred Leitenstorfer, and Davide Bossini**

A Yb:YAG thin-disk regenerative amplifier with 3 kHz repetition rate pumps a second-order nonlinear mixing scheme providing femtosecond transients of maximum electric field strength beyond 330 MV cm^{-1} at a center frequency of 45 THz. This value surpasses field conditions present at submolecular dimensions of matter. The inherent competition between efficiency and bandwidth in parametric downconversion is overcome with a third-order nonlinear step of self-phase modulation (SPM). The high repetition rate, versatility, beam quality, and passive phase stability of our system support advanced spectroscopic approaches like electro-optic sampling (EOS). With this technique, solitonic self-compression and octave-spanning supercontinua directly on a subcycle scale are studied.

1. Introduction

Owing to a broad range of potential applications in both science and technology, the generation of ultrashort and intense light pulses in the mid-infrared (MIR) spectral range is an attractive task. At the same time, it is demanding due to the absence of adequate gain media. The first approaches to generate widely tunable MIR pulses with field amplitudes exceeding 100 MV cm^{-1} rely on difference frequency generation (DFG) driven by two intense pulses in the near-infrared (NIR).[1] A long-wave scheme based on a pump technology at a wavelength of 2 μm has been implemented recently, providing peak field amplitudes of 40 MV cm^{-1} and pulse energies up to 400 μJ in the mid-infrared.[2,3] Such systems open up unprecedented possibilities e.g. in the realm of extreme and off-resonant optical biasing of condensed matter.[4–6] Extension of the cutoff energy of gas-phase high-harmonics generation into the hard X-ray region is enabled by the quadratic scaling of the ponderomotive potential with the driving wavelength.[7–9] Many options exist for resonant nonlinear coupling as the eigenfrequencies of most collective excitations of charges, spins, and the lattice of complex matter reside at MIR frequencies.[10–12] Experiments targeting the control of the coherent dynamics of these eigenmodes demand a field-resolved detection of the MIR laser pulses. Moreover, resonantly driving collective excitations with intense laser pulses would disclose nonlinear dynamics and coupling among degrees of freedom. The hallmark peak intensities for mid-infrared laser technology to disclose unexplored scientific scenarios in solid-state, atomic, and molecular physics are given by the Coulomb fields that arise at both the inter- and intra-atomic levels. They are on the scale of GV cm^{-1}, as determined by the elementary charges of electrons and protons occurring over Å-scale distances.

Recent efforts toward intensive access to the MIR region rely on NIR pump sources combined with nonlinear optical steps for conversion to lower frequencies.[1,13–20] Second- and third-order processes are widely established but both exhibit shortcomings: DFG between two NIR pulses is limited by phase-matching constraints requesting a trade-off between acceptance bandwidth and efficiency due to the finite mismatch of group velocities.[21] On the other hand, SPM in the NIR offers great bandwidth but wavelengths longer than 6 μm are out of reach.[22]

Here, we solve the dilemma between efficiency and acceptance bandwidth by employing a combination of two separate nonlinear processes, namely second-order parametric downconversion followed by spectral broadening based on SPM. This approach results in femtosecond MIR pulses close to GV cm^{-1} electric field strengths comparable with atomic and intra-molecular conditions. At the same time, central frequencies ≈45 THz still allow for straightforward and sensitive subcycle analysis.

2. Difference Frequency Generation Based on Yb:YAG Thin-Disk Technology

A scheme of the experiment is depicted in **Figure 1a**. A regenerative Yb:YAG thin-disk amplifier providing up to 17 mJ of

C. Schoenfeld, L. Feuerer, A.-C. Heinrich, A. Leitenstorfer, D. Bossini
Department of Physics and Center for Applied Photonics
University of Konstanz
D-78457 Konstanz, Germany
E-mail: Davide.Bossini@uni-konstanz.de

The ORCID identification number(s) for the author(s) of this article can be found under https://doi.org/10.1002/lpor.202301152

DOI: 10.1002/lpor.202301152

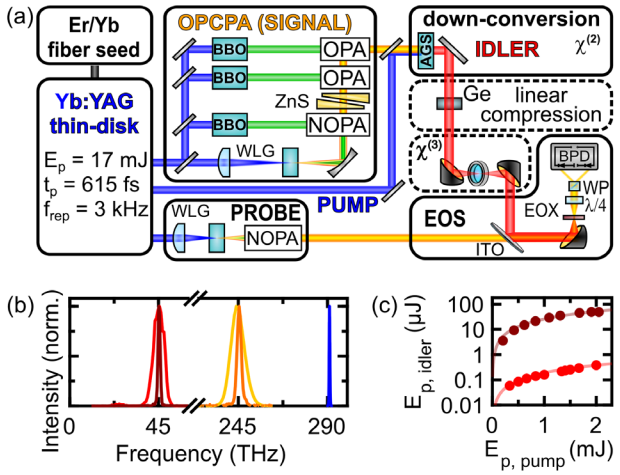

Figure 1. a) Scheme of the experimental setup consisting of an ultrabroadband Er/Yb:fiber frontend, a regenerative sub-ps Yb:YAG thin-disk amplifier, an optical parametric chirped pulses amplifier (OPCPA) seeded by white-light generation (WLG), followed by multi-THz difference frequency generation (DFG) and compression units. The NIR probe pulses are spatially overlapped with the MIR pulses using a broadband beam combiner based on indium tin oxide (ITO) for electro-optic sampling (EOS). This setup includes a GaSe detection crystal (EOX), a quarter-wave plate ($\lambda/4$), a Wollastone prism (WP), and a balanced photodetector (BPD). b) Spectra of the regenerative Yb:YAG thin-disk amplifier (pump; blue), narrow- and broadband examples of OPCPA emission (signal; orange and yellow, respectively) and DFG output (idler; dark red and red graphs) generated in $AgGaS_2$ (AGS). c) MIR pulse energy versus near-infrared pump pulse energy for $AgGaS_2$ crystals with 0.15 mm (red) and 2 mm thickness (dark red). Solid lines represent linear fits to the experimental data according to quantum efficiencies of 0.12% and 20%, respectively.

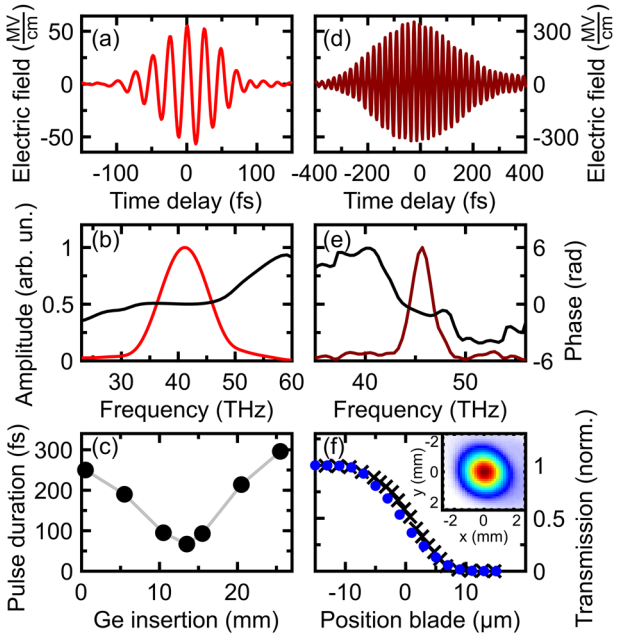

Figure 2. a) Electric-field trace of a MIR pulse generated via DFG in 0.15 mm-thick $AgGaS_2$, temporally compressed via propagation through a 13 mm-thick Ge window and focused to a spot size of 11 μm. b) Corresponding amplitude (red) and phase (black) spectra obtained via Fourier transform. c) MIR pulse duration as a function of the thickness of Ge insertion. d) Electric-field transient of a multicycle MIR pulse generated via DFG in a 2 mm-thick $AgGaS_2$ and focused to a spot size of 11 μm. e) Amplitude and phase spectra corresponding to the time-domain data in (d). f) Transmitted intensity versus position of a knife edge translated along the vertical (blue dots) and horizontal axis (black crosses) for the transient depicted in (d). The resulting spot size is 11 μm (FWHM of the intensity). The inset shows the transverse intensity profile in the far field.

close to transform-limited pulses of 615 fs duration at a center wavelength of 1030 nm (frequency of 291 THz) and repetition rate of 3 kHz with a beam quality of $M^2 = 1.5$ is seeded by a versatile Er/Yb: fiber frontend (Supporting Information S1).[23] Half of this output serves as a pump pulse for subsequent DFG. A second branch is converted to lower frequencies by driving a mJ-class nonlinear optical parametric chirped-pulse amplifier (OPCPA) consisting of white-light generation in YAG and three consecutive amplification stages. Optimum temporal overlap between pump and signal is ensured by a pair of Brewster-angled ZnS wedges for dispersive control of the signal pulse duration after the first stage. Subsequently, both arms are individually expanded to a $1/e^2$ beam diameter of 6 mm and spatially overlapped for collinear type-II DFG in silver gallium sulfide ($AgGaS_2$, AGS) crystals with clear aperture of 8 mm. Passively phase-locked MIR pulses emerge from this approach. $AgGaS_2$ is selected due to its wide band gap of 2.8 eV[24] exceeding the photon energy of 1.2 eV of the pump at 291 THz by more than a factor of two. In this way, losses due to 2-photon absorption are avoided. Figure 1b displays the spectra of all three pulses involved in the nonlinear frequency conversion. The tunable system is exemplary set to generate a MIR transient at 45 THz and is presented for two different configurations of OPCPA and $AgGaS_2$. For a more broadband configuration, we employ type-I β-barium borate (BBO) crystals in all OPCPA stages along with a 0.15 mm-thick $AgGaS_2$ emitter for DFG. The characterization of MIR pulses is accomplished through field-resolved analysis employing EOS. In this technique, the electric field component of the MIR pulse induces refractive index changes in a 17 μm-thick GaSe crystal via the Pockels effect.[1] Measuring the polarization state of the probe beam in a balanced detection scheme, as shown in Figure 1c, while scanning the time delay between both trains of pulses enables to reconstruction of the MIR waveform in the time domain with subcycle resolution. To avoid higher-order nonlinearities and irreversible damage that can result from extreme peak electric field strengths, we use two wire grid polarizers to attenuate the MIR power and deliberately place the GaSe detection crystal far out of focus. The field traces recovered in this way are depicted in **Figure** 2a. Fast Fourier transform reveals amplitude spectra spanning from below 30 to above 55 THz (Figure 2b). The bright red data points in Figure 1c illustrate the MIR pulse energies as a function of pump energy for the DFG. A maximum output energy of 380 nJ is achieved by pumping with 2 mJ, corresponding to an energy conversion efficiency of 0.02 %. On the other hand, the generation of narrowband and highly intense MIR pulses involves type-II BBO crystals in the first two OPA stages and type-I phase matching in the third one, combined with 2 mm-thick $AgGaS_2$. Here, the highest pulse energy (dark red graph in Figure 1c) amounts to 49 μJ, corresponding to an energy conversion efficiency of 2.7 %. Note that in this case, almost 20 %

of pump photons underwent down-conversion during DFG. Degradation of the $AgGaS_2$ surface is observed when the pump energy exceeds 2 mJ, corresponding to a damage threshold of 14 mJ cm^{-2}.

Since the EOS traces in Figure 2 have to be taken with strongly attenuated field amplitudes far out of focus, absolute determination of the confocal electric fields requires exact knowledge of energy densities both in space and time. Under our conditions, total pulse energies readily follow from the average power measured with a thermopile detector and the repetition rate. Relative intensity envelopes may be obtained by squaring the temporal electric field traces from EOS. Depending on the OPCPA configuration and thickness of the $AgGaS_2$ crystal employed, either a few-cycles and broadband (Figure 2a,b) or narrowband multicycle pulses (Figure 2d,e) emerge. The spectral tunability of this system extends across a range from 35 THz to 50 THz, as indicated by the two different central frequencies of 40 THz and 45 THz depicted in Figure 2b,e). Note that the positive chirp of the signal sent by the ZnS wedges is designed to result in negatively chirped MIR pulses after DFG in the $AgGaS_2$ crystal. Therefore, the wave packets may be controlled by simple propagation through a medium with normal dispersion such as germanium. Pulse durations corresponding to the broadband amplitude spectrum in Figure 2b are depicted versus the thickness of antireflection-coated Ge windows used for compression in Figure 2c. The flat phase spectrum in Figure 2b indicates a transform-limited transient with a full-width-at-half-maximum (FWHM) duration of the intensity envelope of 67 fs obtained for a Ge thickness of 13 mm (Figure 2a). Note that the narrowband pulses generated in 2 mm-thick $AgGaS_2$ (Figure 2d,e) directly emerge close to the transform limit and are hardly affected by the Ge insertion. The second information necessary to calculate the electric field amplitude is the confocal intensity distribution of the MIR beam. Ideally, focusing should be as tight as possible since the peak electric field strength scales inversely with the beam waist. We determine this quantity with the knife-edge method after attenuating with a neutral-density filter to prevent ablation of the razor blade. The data set in Figure 2f yields a beam diameter of 11 µm (FWHM of the intensity) focusing with an off-axis parabolic mirror of a focal length of 5 mm. This value is close to the diffraction limit and, in combination with several measurements along the caustic, yields an M^2-value of 1.7. We emphasize that, despite the massive amount of nonlinear optical interactions employed in our setup, this value remains remarkably close to the beam quality of the near-infrared pump. The inset of Figure 2f shows a Gaussian-like and circular transverse mode profile in the far field, as taken with an infrared beam profiling camera (Ophir Sphiricon - Pyrocam IIIHR). Considering the exact temporal waveforms and the spatial energy densities, we calculate a peak amplitude of the electric field of 330 MV cm^{-1} for the narrowband multicycle configuration and 56 MV cm^{-1} for the broadband sub-three-cycle operation, respectively. Notably, a value of 330 MV cm^{-1} corresponds to the Coulomb field at a distance of 2 Å from an elementary point charge ($1.6 \cdot 10^{-19}$ C), comparable e.g. to the atomic radius of elements such as Sr or La[25] or to the bond length of typical molecules such as Cl_2[26].

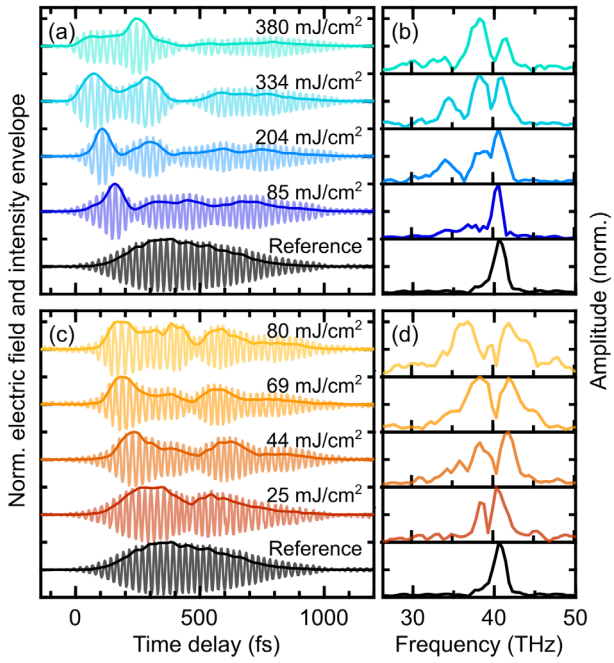

Figure 3. Field-resolved investigation of nonlinear spectral broadening in anomalously dispersive media: Electric-field waveforms (shaded lines) and intensity profile (solid lines), as obtained by electro-optic sampling for increasing incident fluences and after propagation through a) 4 mm of thallium bromo-iodide (KRS-5) and c) 20 mm of KBr. b) and d): Corresponding amplitude spectra, as obtained directly from the time-domain traces via Fourier transform, respectively.

3. Field-Resolved Detection of Third-Order Nonlinear Broadening

Still, our results exploiting second-order conversion suffer from the incompatibility of efficiency and acceptance bandwidth in the DFG process. Assuming no pump depletion, the output energy increases exponentially with the length of the nonlinear medium while the bandwidth decreases with the inverse square root owing to the finite mismatch of group velocities.[21] Here, we overcome this issue by first generating narrowband and intense mid-IR pulses, see Figure 2d,e. We then increase the bandwidth via third-order spectral broadening and solitonic compression. This step requires materials with a broad window of transparency and negative group velocity dispersion (GVD) which are readily available in the MIR. Promising candidates include thallium bromo-iodide (KRS-5), CsI, ZnSe, KBr, and NaCl with corresponding zero-dispersion frequencies of 45, 52, 57, 78, and 109 THz, as calculated from Sellmeier equations.[27–29] The multicycle pulses are focused into the anomalously dispersive sample and recollimated by off-axis parabolic mirrors with focal lengths of 50 mm, yielding a focus spot size of 70 µm (FWHM diameter), see Figure 1a. The MIR fluence is systematically varied to control SPM and to balance its interplay with the anomalous dispersion. All details of the nonlinear pulse propagation, including the solitonic dynamics that arise, are directly accessible on a subcycle level of the electric fields via EOS.

Figure 3a shows the evolution of the field transients and intensity profiles for increasing MIR fluences in a 4 mm-thick KRS-5 crystal with AR coating. Corresponding amplitude spectra are depicted in Figure 3b. For comparison, the black graphs denote the conditions in front of the KRS-5 crystal. At a peak fluence of 85 mJ cm^{-2}, clear evidence of nonlinear dynamics such as pulse splitting and the onset of spectral broadening is observed. Temporal distortions indicate that chromatic dispersion and soliton fission play a pivotal role in the broadening process. By further increasing the MIR fluence and thus the influence of SPM effects, a temporal shock front with a rise time shorter than 100 fs arises because of self-steepening.[30] Beyond this regime, the FWHM of the intensity profile experiences a significant reduction to 100 fs, corresponding to a temporal compression by a factor of four. In comparison with the reference transient, the nonlinear compression scheme enables a potential increase of the peak field by a factor of 1.3, e.g. from 175 to 230 MV cm^{-1} assuming the same transverse intensity distributions and confocal beam diameters of 11 µm. Note that this outcome is achieved despite 40 % of total energy losses owing to residual reflection (2 %) and nonlinear absorption (38 %). Compared to the broadband pulses generated directly by thin $AgGaS_2$ crystals, the temporally compressed intensity profile achieved with the nonlinear compression in KRS-5 in combination with the significantly higher pulse energy is expected to yield a field enhancement of 400 % at comparable bandwidths and confocal spot sizes. Consequently, our approach of combining second- and third-order nonlinear processes to efficiently generate and compress MIR pulses overcomes the limitations associated with the phase mismatch of the DFG process, effectively providing GV cm^{-1} field amplitudes with sub-100 fs pulse duration. We note that a minimum pulse duration together with maximum field amplitudes is mandatory e.g. optimal biasing of condensed matter into exotic states like Wannier-Stark localization because detrimental effects such as off-resonant generation and acceleration of hot charge carriers are minimized. We also observe no signs of long-term degradation in KRS-5, consistent with the literature.[31] In contrast, alkali halides such as NaCl, KBr, and CsI support the formation of color centers for fluences higher than 85 mJ cm^{-2}, severely restricting the use of these materials.[32] To ensure long-term stable operation, we increase the focal length of the off-axis parabola to 100 mm, effectively reducing the confocal intensity by a factor of four. Figure 3c,d shows the field traces and spectral evolution in 20 mm of KBr. Also in this case, we observe significant spectral broadening but without temporal compression due to a finite misbalance between SPM effects and anomalous dispersion. **Figure 4a** summarizes the spectral broadening in KRS-5, CsI, ZnSe, KBr, and NaCl for increasing fluence. The largest bandwidth increase by a factor of 6 is observed with a 20 mm-thick KBr crystal. For SPM-dominated spectral broadening, the nonlinear refractive index n_2 may be determined from.[33]

$$\Delta f \approx \frac{f_0 p_{\max} z}{c t_p A} n_2 \tag{1}$$

where Δf describes the resulting spectral bandwidth, f_0 is the central frequency of incident light, c the speed of light, P_{max} the peak power, A the cross-sectional area at the beam waist, t_p the pulse duration, and z the interaction length which is corresponds to twice the Rayleigh range for the case of free-space focusing. Exploiting Equation (1), we obtain $n_{2,\,KBr} = 3.2{\cdot}10^{-15}$ cm^2 W^{-1} and $n_{2,\,NaCl} = 1.0{\cdot}10^{-15}$ cm^2 W^{-1}, good in agreement with existing literature.[32] A saturation of the spectral broadening is observed in Figure 4a except for KBr and NaCl. Several effects may contribute to this effect: i) nonlinear absorption related to the generation of inverse bremsstrahlung[34] or the dynamic Franz-Keldysh effect[35], ii) limited sensitivity of EOS to frequencies above 55 THz due to the finite bandwidth of our probe pulses and iii) geometrical aspects of the third-order interaction like self-focusing and filamentation. To examine the third point, we study the spatial evolution of the transverse intensity profile in the far field after focusing on KBr and KRS-5 for increasing MIR fluences (Figure 4b). Only minute changes are observed in KBr. In contrast, multi-filamentation appears at 52 mJ cm^{-2} in KRS-5, i.e. at the same intensity where the spectral broadening saturates. This break-up of the transverse mode into many filaments arises due to inhomogeneities in the sample as well as imperfections of the beam profile. If the fluence is further increased, the wavefront collapses and a hot-spot mode emerges at 82 mJ cm^{-2}.

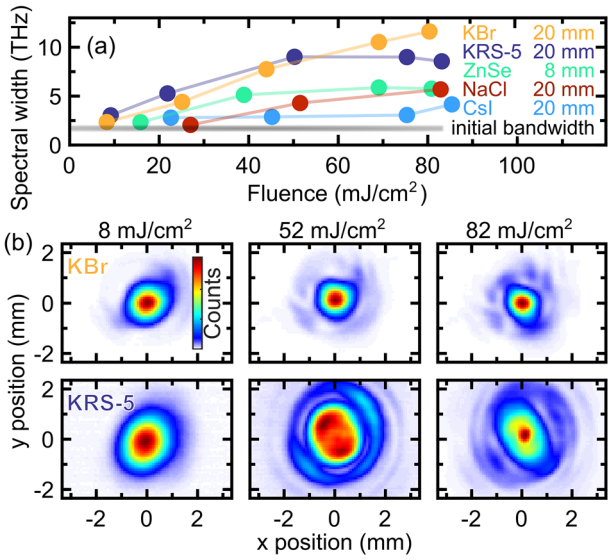

Figure 4. a) Spectral broadening (1/e width) as a function of incident fluence for CsI, KBr, NaCl, ZnSe, and KRS-5 crystals of various thicknesses. The focal length used is 100 mm, resulting in a confocal beam diameter of 155 µm and a Rayleigh length of 8 mm. b) Transverse mode profile in far field after propagation through KBr and KRS-5 with thickness of 20 mm for increasing incident fluence, as taken with an infrared beam profiling camera.

4. Conclusion

In conclusion, we have presented a system for the generation of intense MIR pulses down to the few-cycle regime which combines the high average power supplied by Yb:YAG thin-disk technology with a multi-stage setup for parametric amplification and DFG.

Output pulses of a central frequency of 45 THz reach peak electric field amplitudes of 56 MV cm^{-1} in a broadband sub-three-cycle regime or 330 MV cm^{-1} in a multi-cycle configuration, respectively. These values are comparable to intra-atomic

conditions. The trade-off between bandwidth and efficiency for second-order frequency conversion is avoided by third-order spectral broadening. The passive phase stability and versatility of our setup allow subcycle analysis of the electric field traces via EOS. Consequently, our light source enables a new regime of sensitive investigations of extremely nonlinear and nonperturbative light-matter interactions both under resonant driving of collective resonances and purely off-resonant biasing.

Supporting Information

Supporting Information is available from the Wiley Online Library or from the author.

Acknowledgements

The authors thank A. Baserga, C. Beschle, and S. Eggert for their technical support. This work was supported by Deutsche Forschungsgemeinschaft (SFB 1432, 425217212), Davide Bossini acknowledges the support of the DFG program BO 5074/1-1.

Open access funding enabled and organized by Projekt DEAL.

Conflict of Interest

The authors declare no conflict of interest.

Data Availability Statement

The data that support the findings of this study are available from the corresponding author upon reasonable request.

Keywords

field-resolved supercontinuum generation, frequency conversion, mid-infrared pulse generation, regenerative Yb:YAG thin-disk amplifiers, ultrafast nonlinear optics

Received: November 8, 2023
Revised: February 4, 2024
Published online:

[1] A. Sell, A. Leitenstorfer, R. Huber, *Opt. Lett.* **2008**, *33*, 2767.
[2] P. Fuertjes, L. von Grafenstein, D. Ueberschaer, C. Mei, U. Griebner, T. Elsaesser, *Opt. Lett.* **2021**, *46*, 1704.
[3] P. Fuertjes, M. Bock, L. von Grafenstein, D. Ueberschaer, U. Griebner, T. Elsaesser, *Optica* **2022**, *9*, 1303.
[4] O. Schubert, M. Hohenleutner, F. Langer, B. Urbanek, C. Lange, U. Huttner, D. Golde, T. Meier, M. Kira, S. W. Koch, R. Huber, *Nat. Photonics* **2014**, *8*, 119.
[5] C. Schmidt, J. Bühler, A.-C. Heinrich, J. Allerbeck, R. Podzimski, D. Berghoff, T. Meier, W. G. Schmidt, C. Reichl, W. Wegscheider, D. Brida, A. Leitenstorfer, *Nat. Commun.* **2018**, *9*, 2890.
[6] D. Berghoff, J. Bühler, M. Bonn, A. Leitenstorfer, T. Meier, H. Kim, *Nat. Commun.* **2021**, *12*, 5719.
[7] B. Shan, Z. Chang, *Phys. Rev. A* **2001**, *65*, 011804.
[8] T. Popmintchev, M.-C. Chen, D. Popmintchev, P. Arpin, S. Brown, S. Ališauskas, G. Andriukaitis, T. Balčiunas, O. D. Mücke, A. Pugzlys, A. Baltuška, B. Shim, S. E. Schrauth, A. Gaeta, C. Hernández-García, L. Plaja, A. Becker, A. Jaron-Becker, M. M. Murnane, H. C. Kapteyn, *Science* **2012**, *336*, 1287.
[9] G. Vampa, T. J. Hammond, N. Thiré, B. E. Schmidt, F. Légaré, C. R. McDonald, T. Brabec, P. B. Corkum, *Nature* **2015**, *522*, 462.
[10] M. Först, C. Manzoni, S. Kaiser, Y. Tomioka, Y. Tokura, R. Merlin, A. Cavalleri, *Nat. Phys.* **2011**, *7*, 854.
[11] T. F. Nova, A. Cartella, A. Cantaluppi, M. Först, D. Bossini, R. V. Mikhaylovskiy, A. V. Kimel, R. Merlin, A. Cavalleri, *Nat. Phys.* **2017**, *13*, 132.
[12] A. Stupakiewicz, C. S. Davies, K. Szerenos, D. Afanasiev, K. S. Rabinovich, A. V. Boris, A. Caviglia, A. V. Kimel, A. Kirilyuk, *Nat. Phys.* **2021**, *17*, 489.
[13] R. Huber, A. Brodschelm, F. Tauser, A. Leitenstorfer, *Appl. Phys. Lett.* **2000**, *76*, 3191.
[14] D. Brida, C. Manzoni, G. Cirmi, M. Marangoni, S. Bonora, P. Villoresi, S. D. Silvestri, G. Cerullo, *J Opt* **2009**, *12*, 013001.
[15] G. Andriukaitis, T. Balčiūnas, S. Ališauskas, A. Pugžlys, A. Baltuška, T. Popmintchev, M.-C. Chen, M. M. Murnane, H. C. Kapteyn, *Opt. Lett.* **2011**, *36*, 2755.
[16] C. Gaida, M. Gebhardt, T. Heuermann, F. Stutzki, C. Jauregui, J. Antonio-Lopez, A. Schülzgen, R. Amezcua-Correa, A. Tünnermann, I. Pupeza, J. Limpert, *Light Sci Appl* **2018**, *7*, 94.
[17] U. Elu, L. Maidment, L. Vamos, F. Tani, D. Novoa, M. H. Frosz, V. Badikov, D. Badikov, V. Petrov, P. St. J. Russell, J. Biegert, *Nat. Photonics* **2021**, *15*, 277.
[18] M. Seidel, X. Xiao, S. A. Hussain, G. Arisholm, A. Hartung, K. T. Zawilski, P. G. Schunemann, F. Habel, M. Trubetskov, V. Pervak, O. Pronin, F. Krausz, *Sci. Adv.* **2018**, *4*, eaaq1526.
[19] O. Novák, P. R. Krogen, T. Kroh, T. Mocek, F. X. Kärtner, K.-H. Hong, *Opt. Lett.* **2018**, *43*, 1335.
[20] B.-H. Chen, E. Wittmann, Y. Morimoto, P. Baum, E. Riedle, *Opt. Express* **2019**, *27*, 21306.
[21] C. Manzoni, G. Cerullo, *J Opt* **2016**, *18*, 103501.
[22] K. L. Vodopyanov, *Laser-Based Mid-Infrared Sources and Applications*, John Wiley & Sons, Hoboken, NJ, USA, **2020**.
[23] J. Fischer, A.-C. Heinrich, S. Maier, J. Jungwirth, D. Brida, A. Leitenstorfer, *Opt. Lett.* **2016**, *41*, 246.
[24] F. Rotermund, V. Petrov, F. Noack, *Opt. Commun.* **2000**, *185*, 177.
[25] J. C. Slater, *J. Chem. Phys.* **1964**, *41*, 3199.
[26] D. R. Lide, *CRC Handbook of Chemistry and Physics*, 85th ed., CRC Press, Boca Raton, FL, USA, **2004**.
[27] W. S. Rodney, I. H. Malitson, *JOSA* **1956**, *46*, 956.
[28] H. H. Li, *J. Phys. Chem. Ref. Data* **1976**, *5*, 329.
[29] T. Amotchkina, M. Trubetskov, D. Hahner, V. Pervak, *Appl. Opt.* **2020**, *59*, A40.
[30] G. P. Agrawal, *Phys. Rev. A* **1991**, *44*, 7493.
[31] A. Marcinkevičiūtė, G. Tamošauskas, A. Dubietis, *Opt. Mater.* **2018**, *78*, 339.
[32] A. Marcinkevičiūtė, V. Jukna, R. Šuminas, N. Garejev, G. Tamošauskas, A. Dubietis, *Results Phys* **2019**, *14*, 102396.
[33] R. W. Boyd, in *Nonlinear Opt. Third Ed*, (Ed.: R. W. Boyd), Academic Press, Burlington **2008**, 329.
[34] A. Couairon, A. Mysyrowicz, *Phys. Rep.* **2007**, *441*, 47.
[35] A. H. Chin, J. M. Bakker, J. Kono, *Phys. Rev. Lett.* **2000**, *85*, 3293.